THE JOURNAL OF PHYSICAL CHEMISTRY C

Article

pubs.acs.org/JPCC

Second Harmonic and Sum-Frequency Generation from Aqueous Interfaces Is Modulated by Interference

Grazia Gonella,[†,#] Cornelis Lütgebaucks,[‡,#] Alex G. F. de Beer,[‡] and Sylvie Roke*[,‡]

[†]Max Planck Institute for Polymer Research, Ackermannweg 10, 55128 Mainz, Germany

[‡]Laboratory for fundamental BioPhotonics (LBP), Institute of Bioengineering (IBI), and Institute of Materials Science (IMX), School of Engineering (STI), and Lausanne Centre for Ultrafast Science (LACUS), École Polytechnique Fédérale de Lausanne (EPFL), CH-1015 Lausanne, Switzerland

Supporting Information

ABSTRACT: The interfacial region of aqueous systems also known as the electrical double layer can be characterized on the molecular level with second harmonic and sum-frequency generation (SHG/SFG). SHG and SFG are surface specific methods for isotropic liquids. Here, we model the SHG/SFG intensity in reflection, transmission, and scattering geometry taking into account the spatial variation of all fields. We show that, in the presence of a surface electrostatic field, interference effects, which originate from oriented water molecules on a length scale over which the potential decays, can strongly modify the probing depth as well as the expected intensity at ionic strengths $<10^{-3}$ M. For reflection experiments this interference phenomenon leads to a significant reduction of the SHG/SFG intensity. Transmission mode experiments from aqueous interfaces are hardly influenced. For SHG/SFG scattering experiments the same interference leads to an increase in intensity and to modified scattering patterns. The predicted scattering patterns are verified experimentally.

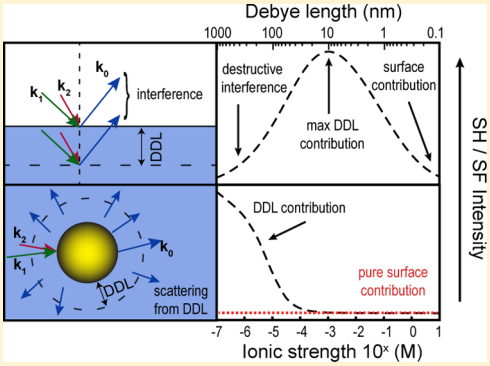

INTRODUCTION

Ions modify the structure and dynamics of water. In contact with an interfacial region, ions change the physical, chemical, electrostatic, and biochemical properties of a material.[1−4] Quantifying the molecular properties of the electrical double layer (EDL), which consists of the interface itself as well as the diffuse EDL, is important for many processes in biology and chemistry. Many methods exist for this purpose: employing electrokinetic mobility,[5,6] scattered or reflected, visible or X-ray photons and neutrons,[7,8] vibrational spectroscopy,[2,4,9] photoelectron spectroscopy,[10] and nonlinear optical methods, such as second harmonic and sum-frequency generation (SHG/SFG).[11−16] What all of these methods have in common, and what considerably complicates the interpretation of data and the formulation of a consistent molecular level picture of the EDL, is that the interfacial region and its thickness can be chosen in different ways.[17−21] The interfacial thickness typically depends on the sensitivity, the background, and penetration depth of the method. SHG and SFG are background free methods, and the probing depth is determined by a requirement of spatial noncentrosymmetry of the material: The interface is commonly defined as that region where centrosymmetry is broken, provided that it is located between isotropic media.[22] SHG and SFG are thus ideal methods for probing molecular level details of the aqueous interface, which is considered to be only a few molecular dimensions thick (see refs 2, 4, 9, 12, and 14 for excellent reviews). However, when an (electrolyte dependent) electrostatic field is present in the interfacial region, water molecules in the EDL reorient (even if they are isotropically distributed in absence of an electrostatic field). This results in a small amount of centrosymmetry breaking, leading to an additional contribution to the nonlinear optical response.[17,20,23] This effect changes the interfacial thickness that is probed in the experiment. At the same time the optical beams vary in phase as they propagate in the aqueous phase, which may result in interference effects with the spatially varying electrostatic field. Does this influence the probing depth, and does it depend on electrolyte concentration? Can we still assume that the first few molecular diameters at the interface are probed? The interpretation of SHG and SFG experiments needs to take these factors into account.

Here, we consider these questions, following the trend set by various previous studies.[2,14,20,21,24−26] We take into account the ionic strength range from 10^{-7} to 10 M and derive a theoretical expression for the SHG/SFG response. We calculate the SHG and SFG response from an aqueous planar interface in reflection and transmission geometry and an aqueous colloidal interface in scattering geometry. On the basis of our findings, it turns out that the probing depth into the bulk solution varies with ionic strength and that, in certain experimental conditions, it can be >1 μm. Within this >1 μm thick region, interference effects between photons that are generated at different

Received: December 20, 2015
Revised: April 4, 2016
Published: April 5, 2016

DOI: 10.1021/acs.jpcc.5b12453
J. Phys. Chem. C 2016, 120, 9165−9173

distances away from the Gibbs dividing surface of the interface alter the expected intensity considerably. Assuming an ionic strength independent second-order susceptibility, for reflection mode experiments this may result in a significantly decreased intensity at low ionic strengths than what one would expect. Furthermore, the interference at low ionic strengths effectively reduces the probing depth, which, in the limit of an infinite Debye length, is reduced back to the interfacial region that would be probed in absence of an electrostatic field. For transmission experiments this effect is largely absent. For nonresonant angle-resolved scattering[27−29] experiments, the equations that describe the emitted intensity are derived, which are distinctly different from the reflection and transmission equations. Here, the contribution from the diffuse EDL increases the intensity and strongly modifies the scattering patterns, which allows for a separation of the surface signal from that of the diffuse EDL.

In what follows we first describe reflection and transmission mode experiments, considering a theoretical background to which we add the expected changes when interference occurs. We describe the result in terms of probing depth and make a comparison to previous reflection mode studies in the literature. In the second part we describe the theoretical background (using the Rayleigh-Gans-Debye approximation) for second harmonic and sum-frequency scattering and adapt the formalism to incorporate scattering form the diffuse EDL. We examine the probing depth and provide an experimental verification of the found expressions.

RESULTS AND DISCUSSION

SHG/SFG in Reflection Mode. *Theoretical Background.* In the electric-dipole approximation, in an SFG process two optical fields $\mathbf{E}_1(\omega_1) = E_1(\omega_1, k_1)\boldsymbol{u}_1 = E_1(\omega_1)e^{-i(\omega_1 t - \mathbf{k}_1\mathbf{r})}\boldsymbol{u}_1$ and $\mathbf{E}_2(\omega_2) = E_2(\omega_2, k_2)\boldsymbol{u}_2 = E_2(\omega_2)e^{-i(\omega_2 t - \mathbf{k}_2\mathbf{r})}\boldsymbol{u}_2$ with wave vectors and frequencies $\mathbf{k}_1$, ω_1 and $\mathbf{k}_2$, ω_2 interact with an interface that is characterized by a surface second-order susceptibility $\chi_s^{(2)}(\omega_0 = \omega_1 + \omega_2)$. For SHG, $\omega_1 = \omega_2$ and $\mathbf{k}_1 = \mathbf{k}_2$. The second-order nonlinear optical polarization $\mathbf{P}^{(2)}(\omega_0)$ that results from the interaction of the beams with the interfacial region is

$$\mathbf{P}^{(2)}(\omega_0) = \varepsilon_0 \chi_s^{(2)} : \mathbf{E}_1(\omega_1)\mathbf{E}_2(\omega_2) \quad (1)$$

Surface charges and ions in solution generate an additional electrostatic field. For a reflection mode experiment with the interface placed at $z = 0$ (Figure 1a), we thus have $\mathbf{E}(\omega = 0, z) = \mathbf{E}_{DC}(z)$, which generates an additional interaction term in the nonlinear polarization:[26,30−33]

$$\mathbf{P}_{NL}(\omega_0) = \mathbf{P}^{(2)}(\omega_0) + \mathbf{P}^{(3)}(\omega_0) + \ldots \text{ with}$$

$$\mathbf{P}^{(3)}(\omega_0) = \int_0^{+\infty} \mathbf{P}^{(3)}(\omega_0, z)\, dz \text{ and}$$

$$\mathbf{P}^{(3)}(\omega_0, z) = \varepsilon_0 \chi^{(3)\prime} : \mathbf{E}_1(\omega_1)\mathbf{E}_2(\omega_2)\mathbf{E}_{DC}(z) \quad (2)$$

Here, $\chi^{(3)\prime}$ is an effective third-order susceptibility tensor. $\chi^{(3)\prime}$ represents all processes that lead to emission at ω_0 and that require an interaction with $\mathbf{E}_{DC}(z)$. This includes $\mathbf{E}_{DC}$-oriented water molecules at the interface and in the bulk solution as well as a pure third-order interaction that is mediated by the isotropic third-order susceptibility of bulk water $\chi_b^{(3)}$. $\mathbf{P}^{(3)}(\omega_0, z)$ is a function of z, because the electrostatic field changes in the direction perpendicular to the interface. The total $\mathbf{P}^{(3)}(\omega_0)$ polarization is obtained by an integration over z.[17] With the assumption of isotropy in the x and y directions, the amplitude of $\mathbf{P}^{(3)}(\omega_0)$ reads

$$P^{(3)}(\omega_0) = \varepsilon_0 \int_0^{+\infty} \chi^{(3)\prime} E_1(\omega_1, k_1)E_2(\omega_2, k_2)E_{DC}(z)\, dz \quad (3)$$

Integrating, one obtains

$$P^{(3)}(\omega_0) \propto \varepsilon_0 \chi^{(3)\prime} E_1(\omega_1, k_1)E_2(\omega_2, k_2) \int_0^{+\infty} E_{DC}(z)\, dz = \varepsilon_0 \chi^{(3)\prime} E_1(\omega_1, k_1)E_2(\omega_2, k_2)\Phi_0 \quad (4)$$

where Φ_0 represents the surface potential.

Interference and the Diffuse EDL. Provided one knows the relationship between Φ_0, the ionic strength (c), and the surface charge (σ_0), eq 4 allows the estimation of the surface potential Φ_0 by the Eisenthal $\chi^{(3)}$-method, utilizing a series of reflection mode experiments performed at different ionic strengths.[14,17,26]

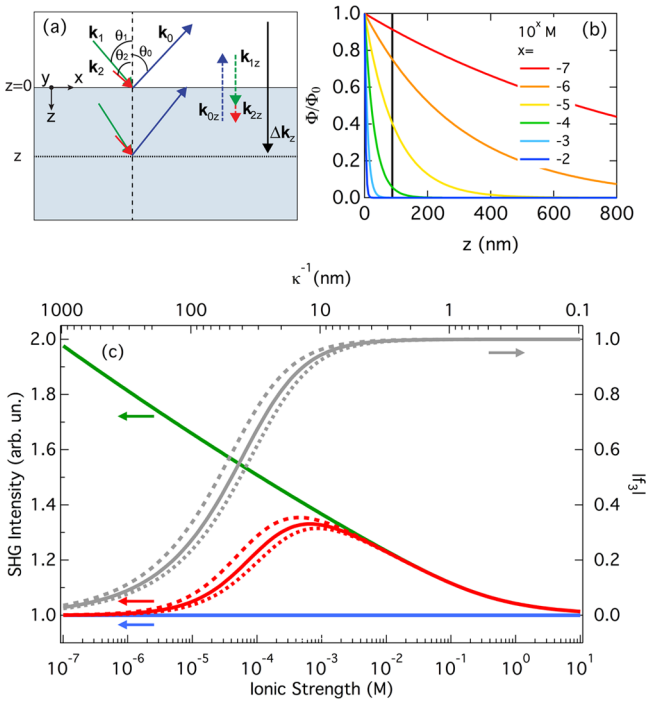

Figure 1. (a) Geometry of an SFG reflection experiment at the air/water interface. Arrows $\mathbf{k}_1$, $\mathbf{k}_2$, and $\mathbf{k}_0$ refer to the visible, IR, and sum-frequency beams that can interact at various z-planes. The dashed arrows refer to their projection along the z-axis, and the relevant phase difference. Δk_z is also illustrated. For collinear SHG $\mathbf{k}_1 = \mathbf{k}_2$. (b) Exponentially decaying electrostatic potentials of the form $\Phi(z) = \Phi_0 e^{-\kappa z}$ for ionic strengths of (red) 10^{-7}, (orange) 10^{-6}, (yellow) 10^{-5}, (green) 10^{-4}, (cyan) 10^{-3}, (blue) 10^{-2} M. The black line indicates the distance $z = 88$ nm where, in the current geometry, $\Delta k_z z = \pi$. (c) Calculated SHG intensity (left axis) as a function of ionic strength taking into account the following: Blue line: only $\chi_s^{(2)}$, using eqs 1 and 9a, green line: $\chi_s^{(2)}$ and $\chi^{(3)\prime}$ contribution, using eqs 4 and 9a, and red line: both effects together with the interference term $f_3(\kappa, \Delta k_z)$ using eq 9b. The magnitude of the correction factor $|f_3(\kappa, \Delta k_z)|$ (right axis) as a function of ionic strength is also shown (gray line). We used the following parameters: $|\chi_s^{(2)}| = 1$, $|\chi^{(3)\prime}| = -1$, $\theta_1 = \theta_2 = 45°$, $\lambda_1 = \lambda_2 = 800$ nm, $n_{air} = 1$, n_{H_2O} (800 nm) = 1.33, and n_{H_2O} (400 nm) = 1.34. The dotted (dashed) line corresponds to curves calculated for $\theta_1 = \theta_2 = 10°$ ($\theta_1 = \theta_2 = 80°$). The $|\chi_s^{(2)}| = 1$, $|\chi^{(3)\prime}| = -1$ values also take into account the Fresnel factors. $|\chi_s^{(2)}|$ and $|\chi^{(3)\prime}|$ were taken from published data of air−water interfaces.[31,35−37]

DOI: 10.1021/acs.jpcc.5b12453
J. Phys. Chem. C 2016, 120, 9165−9173

Equation 4 assumes that the optical fields are independent of z, meaning that the phases of the incoming and returning fields do not change in the region where E_{DC} is nonzero. The validity of this assumption can be estimated by comparing the z-dependent decay of the electrostatic potential $\Phi(z)$ to the phase change of the generated SHG/SFG field originating from different z-planes. For a planar surface with an electrostatic potential that decays as $e^{-\kappa z}$, in which κ^{-1} is the Debye length, the potential has decayed to 2% of its maximum value at $z = 4\kappa^{-1}$ (Figure 1b). The wave vector mismatch for SHG/SFG photons generated at different probing depths is $\Delta k_z = |\mathbf{k}_{1z} + \mathbf{k}_{2z} - \mathbf{k}_{0z}| = k_{1z} + k_{2z} + k_{0z}$ with $k_{iz} = \omega_i/c\sqrt{n(\omega_i)^2 - \sin(\theta_i)^2}$ using $n(\omega_i)$ for the refractive index and θ_i for the angle between the incoming $\mathbf{k}_i$-vector and the surface normal in air for each beam i (sketched in Figure 1a). For an experiment performed at the air/water interface with parameters $\theta_{1,2} = 45°$, $\lambda_1 = \lambda_2 = 800$ nm, the phase change of the generated SHG beam reaches a value of π at $z = 88$ nm ($\pi\Delta k_z^{-1} = 88$ nm, the black line in Figure 1b). Thus, at ionic strengths for which $\mathbf{E}_{DC}$ is insufficiently screened to still be present beyond $\pi\Delta k_z^{-1}$ we can expect that eq 4 becomes invalid, and we have to incorporate a z-dependence in the optical beams of eq 3. From Figure 1b it can be estimated that this will be the case if $c \lesssim 10^{-3}$ M. We then obtain

$$P^{(3)}(\omega_0) = \varepsilon_0 \int_0^{+\infty} \chi^{(3)'} E_1(\omega_1, k_1) E_2(\omega_2, k_2) E_{DC}(z) e^{i\Delta k_z z}\, dz \tag{5}$$

which is identical to

$$P^{(3)}(\omega_0) = \varepsilon_0 \chi^{(3)'} E_1(\omega_1) E_2(\omega_2) \int_0^{+\infty} \left(-\frac{d}{dz}\Phi(z)\right) e^{i\Delta k_z z}\, dz \tag{6}$$

using $E_{DC}(z) = -\frac{d}{dz}\Phi(z)$. Integration by parts of the integral in eq 6 returns the following expression:

$$P^{(3)}(\omega_0) = \varepsilon_0 \chi^{(3)'} E_1(\omega_1) E_2(\omega_2)(\Phi_0 + i\Delta k_z \int_0^{+\infty} \Phi(z) e^{i\Delta k_z z}\, dz) \tag{7}$$

The second term requires an analytical expression for $\Phi(z)$. Since this part only contributes to the expression several nanometers away from the interface, we can use for $\Phi(z)$ the diffuse double layer (DDL) equation $\Phi(z) = \Phi_0 e^{-\kappa z}$, without loss of generality. Note that this also means that the integral in eq 7 does not contribute to the polarization at ionic strengths $>10^{-2}$ M. Thus, in this range, the result will not depend on the functional form chosen to describe $\Phi(z)$. Substituting the DDL equation and integrating, we obtain

$$P^{(3)}(\omega_0) = \varepsilon_0 \chi^{(3)'} E_1(\omega_1) E_2(\omega_2) \Phi_0 \frac{\kappa}{\kappa - i\Delta k_z} = \varepsilon_0 \chi^{(3)'} E_1(\omega_1) E_2(\omega_2) \Phi_0 f_3(\kappa, \Delta k_z) \tag{8}$$

Finally, the emitted intensity is

$$I(\omega_0) \propto |P^{(2)}(\omega_0) + P^{(3)}(\omega_0)|^2 \tag{9a}$$

$$I(\omega_0) \propto I_1(\omega_1) I_2(\omega_2) \left| \chi_s^{(2)} + \chi^{(3)'} \Phi_0 \frac{\kappa}{\kappa - i\Delta k_z} \right|^2 \tag{9b}$$

Note that the appropriate tensor elements for $\chi_s^{(2)}$ and $\chi^{(3)'}$, and Fresnel coefficients need to be inserted and depend on the polarization combination used.[34] Note also that in the present derivation $\chi_s^{(2)}$ is considered constant; that is, this derivation does not take any chemical changes into account.

The magnitude of the correction term $f_3(\kappa, \Delta k_z) = \frac{\kappa}{\kappa - i\Delta k_z}$ is plotted in Figure 1c (right axis) for a collinear ($\boldsymbol{k}_1 = \boldsymbol{k}_2$) SHG reflection experiment using $\lambda_1 = \lambda_2 = 800$ nm, $\theta_{1,2} = \theta_0 = 45°$, $|\chi_s^{(2)}| = 1$, and $|\chi^{(3)'}| = -1$, values close to derived numbers from published experiments.[31,35−37] Since Φ_0 typically depends on the ionic strength, we use here[38] (for illustration purposes only) $\Phi_0 = \frac{2k_BT}{e}\sinh^{-1}\left(\frac{\sigma_0}{\sqrt{8000 k_B T N_A c \varepsilon_0 \varepsilon_r}}\right)$ for a 1:1 electrolyte with a surface charge density $\sigma_0 = -0.05$ C/m^2. As can be seen for $c > 10^{-3}$ M, $\kappa^{-1} \ll \Delta k_z^{-1}$, and $f_3(\kappa, \Delta k_z) \to 1$, in agreement with eq 4.[17] Figure 1c also displays the calculated emitted SHG intensity (left axis) considering three relevant functions: (1) the potential independent $\chi_s^{(2)}$ intensity according to eqs 1 and 9a (blue line), (2) the intensity originating from both the $\chi_s^{(2)}$ and $\chi^{(3)'}$ contribution according to eqs 4 and 9a (green line), and (3) the intensity originating from both the $\chi_s^{(2)}$ and $\chi^{(3)'}$ contribution excited with optical fields that vary along the z-direction (red line, eq 9b). For this calculation the value of $\chi_s^{(2)}$ was approximated from refs 31 and 35−37, which deal with nonresonant SHG from air/water interfaces. It can be seen that the $\chi_s^{(2)}$ contribution (blue line) to the total intensity, which neglects possible electrostatic field induced reorientation of interfacial water molecules, does not depend on the ionic strength as it does not depend on Φ_0. The combined z-independent $\chi_s^{(2)}$ and $\chi^{(3)'}$ contribution (green line) strongly depends on the ionic strength, and keeps increasing as the ionic strength is lowered. When the z-dependence of all fields is considered (eq 9b, red line), the intensity does not increase below $\sim 10^{-3}$ M, but drops back to the level of the $\chi_s^{(2)}$-only contribution.

Probing Depth. The trend of the red line in Figure 1c can be understood considering the following effects: At ionic strengths $>10^{-1}$ M, $\chi_s^{(2)}$ is mainly responsible for the SHG signal as $4\kappa^{-1}$ involves only a few layers of water molecules, and the effect of reorientation by an electrostatic field is generally smaller than other effects.[39] Decreasing the ionic strength from 10^{-1} to 10^{-3} M increases the number of water molecules that are influenced by the electrostatic field (up to a distance of $4\kappa^{-1} \simeq 36$ nm, involving ∼120 "layers" of water molecules). This increase in screening depth increases the SHG signal by ∼35% for the case of susceptibility elements with equal magnitudes plotted in Figure 1c.[20] Between 10^{-3} and 10^{-4} M, $4\kappa^{-1} \simeq \pi\Delta k_z^{-1}$. Below 10^{-4} M, $4\kappa^{-1} \gg \pi\Delta k_z^{-1}$. SHG photons are generated at different z-planes within the $4\kappa^{-1}$ region, that may extend up to ∼4000 nm at 10^{-7} M, involving 13 000 "layers" of water molecules. The interferences of the reflected SHG photons generated at different planes is, however, destructive and reduces the SHG intensity even though the probing depth is increased. Once $\kappa^{-1} \gg \Delta k_z^{-1}$ (or $\kappa \ll \Delta k_z$), there is complete destructive interference, and only the $\chi_s^{(2)}$ contribution to the intensity is left. Thus, although the probing depth may be very deep, the destructive nature of the interference brings back the interfacial specificity. We will see when we consider a transmission geometry and a scattering geometry from a

DOI: 10.1021/acs.jpcc.5b12453
J. Phys. Chem. C 2016, 120, 9165−9173

particle that this is a purely geometrical effect. We will also see that the present expression cannot be used to describe a scattering process.

Comparison to Existing Literature. With the consideration that many SFG studies aimed at probing the EDL as a function of ionic strength or pH (see, e.g., the overviews of refs 40−43) generally employ the framework of eqs 4 and 9a, the above analysis has significant consequences for the way the interface is described. Often it is observed that adding an electrolyte (or changing the pH) causes a big increase in the intensity compared to an electrolyte free condition. This response can then be interpreted to result from a large free energy for ionic absorption. However, Figure 1c shows that if one relies on an interpretation that is based on eqs 4 and 9a, the expected ion induced change is much larger than the change obtained by eq 9b. Figure 1c shows that, according to the green curve, increasing the ionic strength from 10^{-7} to 10^{1} M results in a decrease in the intensity by a factor of 2. Note that this magnitude depends on the surface potential, and can be much bigger (as we have assumed a relatively low charge density). According to the red curve, however, the intensities at 10^{-7} and 10^{1} M are approximately identical (although for different reasons). This effectively implies that, when we correct for interference, ions are not nearly as strongly surface specific as expected. The described behavior can very well explain the SHG intensity change observed by the Geiger lab[44] at the fused silica/water interface as a function of indifferent electrolyte concentration (NaCl). This study by Achtyl et al. reports an electrolyte dependent intensity that closely resembles the red line in Figure 1c (and not the green line). Rather than requiring ion adsorption or surface modification at very low ionic strengths, the SH intensity deviates from the green line because it reports on the interference between photons generated in the bulk of the diffuse EDL and the surface structure. Also, the dependence of the SFG intensity on ionic strength measured at the fused silica/water interface reported by the Hore lab[20] deviates strongly from the behavior expected on the basis of eq 4. Instead of a sharply increasing intensity with low ionic strength, the data levels off at ionic strengths <0.7 mM and shows similarities to the data in Figure 1c. Although the interpretation in this work is similar to the interpretation of ref 20 for $c > 10^{-3}$ M, for $c < 10^{-3}$ M it is different: The probing depth is not limited by the coherence length. Rather, in the case of a decaying electrostatic field, the $\chi^{(3)\prime}$ term is z-dependent and will continue contributing over distances beyond the coherence length. The z-dependence effectively increases the $\chi^{(3)\prime}$ contribution and would modify the presented solution in ref 20 with one that does not require a concentration dependence of the bulk $\beta^{(3)}$ or $\beta^{(2)}$ term and a smaller adjustment in the $\chi_s^{(2)}$ contribution. It is also worth noting that a correction in the charge density may have been needed as this was taken from the literature and not measured.

Another set of studies in refs 18, 45, and 46 reports on an increase in the resonant SFG intensity as a function of increasing pH on the octadecyltrichlorosilane (OTS)/water interface[18,46] and the PDMS/water interface.[45] On the basis of this increase for negatively charged surfaces at pH > 7, it was concluded[18] that hydroxide ions have unusually high surface affinities for hydrophobic interfaces, and this was used to derive a free energy of absorption of 45 kJ/mol (18 kT per molecule). In these studies it can be seen that, as the pH is increased from 7 to 14[45] or 11,[18] a maximum SFG intensity is reached at pH 10/11, i.e., at an ionic strength of $10^{-4}/10^{-3}$ M. This corresponds to the trend plotted in Figure 1c. It is therefore probably more meaningful to explain the strong pH dependence as mainly originating from interference, instead of only being caused by the adsorption of OH^-. Two further arguments can be made in favor of the presented interpretation. Many experimental and theoretical studies have considered the possible surface propensity of hydroxide ions, and the majority of these studies did not find a large surface affinity of OH^- ions (reviewed in ref 47). In addition, Tian et al.[18] report in the same work a comparable trend for NaCl (although this is limited only to ionic strengths up to ∼30 μM, which would correspond to a pH of ∼9.5).

SHG/SFG in Transmission Mode. Next, we consider briefly the case for a transmission mode geometry. The treatment for SHG and SFG in transmission geometry closely follows the one in reflection geometry, and eqs 1−9 are still valid. The fundamental difference is in the expression for Δk_z. In fact, in this geometry and away from resonances $\Delta k_z = |\mathbf{k}_{1z} + \mathbf{k}_{2z} - \mathbf{k}_{0z}| = k_{1z} + k_{2z} - k_{0z}$ returns bigger values for Δk_z^{-1} compared to the reflection geometry. Using the same incident parameters as for the reflection geometry, namely, a collinear ($\mathbf{k}_1 = \mathbf{k}_2$) geometry using $\lambda_1 = \lambda_2 = 800$ nm, $\theta_{1,2} = 45°$, n_{H_2O} (800 nm) = 1.33, and n_{H_2O} (400 nm) = 1.34, in transmission we obtain $\Delta k_z^{-1} \cong 5.4$ μm. Hence, in transmission geometry, for a 1:1 electrolyte, in order to have $4\kappa^{-1} > \pi\Delta k_z^{-1}$, an ionic strength $c < 1.7 \times 10^{-12}$ M is needed. This means that in the whole experimentally accessible range $|f_3(\kappa, \Delta k_z)| \rightarrow 1$. In other words, eq 4 provides a good description of SHG/SFG in transmission geometry at any ionic strength. In Figure 2a $|f_3(\kappa, \Delta k_z)|$ as calculated in transmission geometry (left axis) is reported as a function of the ionic strength and compared to the one in reflection mode (right axis, same geometry as in Figure 1c). Note that as far as we are aware no transmission experiments have been conducted. For comparison, in panel b, $|F_3(\kappa R, qR)|/(4\pi R^2)$ as calculated in scattering geometry is reported as a function of ionic strength and will be discussed later.

SHG/SFG in Scattering Mode. *Theoretical Background.* The above considerations are equally important for the analysis of the EDL of particles, droplets, vesicles, and other colloids in aqueous solution. In what follows we develop the formalism to describe sum-frequency scattering (SFS) and second harmonic scattering (SHS). It is anticipated that a different geometry will lead to expressions that are distinctly different from the ones derived for transmission and reflection geometry (eqs 8 and 9). Figure 3a shows the top view of a SF scattering experiment. Here θ is the scattering angle, which is defined as the angle between the wave vector of the scattered (detected) light $\mathbf{k}_0$, and the sum of the incoming wavevectors $\mathbf{k}_1$ and $\mathbf{k}_2$. The opening angles α and β are defined as shown in Figure 3a.

The scattering wave vector $\mathbf{q}$ is defined as $\mathbf{q} \equiv \mathbf{k}_0 - (\mathbf{k}_1 + \mathbf{k}_2)$. For collinear SHS, $\mathbf{k}_1 = \mathbf{k}_2$ and $\omega_1 = \omega_2$. As shown previously,[48,49] in absence of surface charges the scattered second harmonic intensity is given by

$$I(\omega_0) = 2n(\omega_0)\sqrt{\varepsilon_0/\mu_0}\,|\mathbf{E}(\omega_0)|^2 \tag{10}$$

where $n(\omega_0)$, ε_0, μ_0 are the refractive index, vacuum permittivity, and permeability, respectively.

The amplitude of the scattered SF/SH field $E_{ijk}(\omega_0)$ can be expressed as[50]

DOI: 10.1021/acs.jpcc.5b12453
J. Phys. Chem. C 2016, 120, 9165−9173

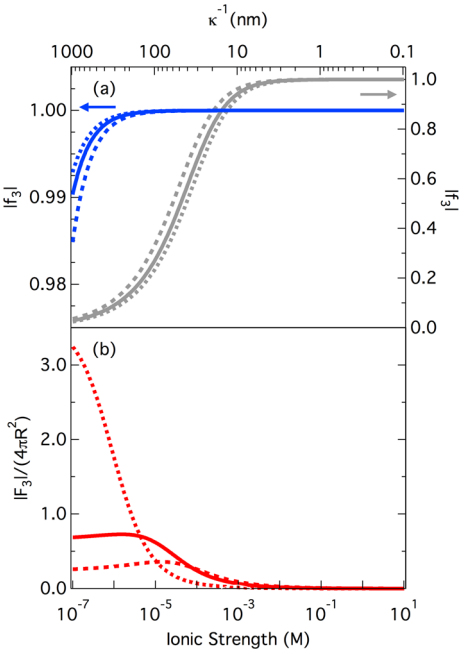

Figure 2. (a) $|f_3(\kappa, \Delta k_z)|$ in transmission geometry (blue continuous curve, left axis) and reflection geometry (gray continuous curve, right axis), as a function of ionic strength. We used the following input values: $\theta_1 = \theta_2 = 45°$, $\lambda_1 = \lambda_2 = 800$ nm, $n_{air} = 1$, $n_{H_2O}(800\text{ nm}) = 1.33$, and $n_{H_2O}(400\text{ nm}) = 1.34$. The dotted (dashed) line corresponds to curves calculated for $\theta_1 = \theta_2 = 10°$ ($\theta_1 = \theta_2 = 80°$). (b) $|F_3(\kappa R, qR)|/(4\pi R^2)$ for a scattering geometry calculated as a function of ionic strength c. We used the following as parameters: $\theta = 45°$, $\lambda_1 = \lambda_2 = 1028$ nm, $n_{air} = 1$, $n_{H_2O}(1028\text{ nm}) = 1.33$, and $n_{H_2O}(514\text{ nm}) = 1.33$, and $R = 50$ nm. The continuous, dotted, and dashed lines correspond to curves calculated at scattering angles $\theta = 45°$, 10°, and 80°, respectively.

$$E_{ppp}(\omega_0) = \frac{ick_0^2}{2\pi|\hat{r}||\hat{I}|}\frac{e^{ik_0r_0}}{r_0}E_1(\omega_1)E_2(\omega_2)\left[\cos\left(\frac{\theta}{2}\right)\cos\left(\frac{\theta}{2}-\alpha\right)\cos\left(\frac{\theta}{2}-\alpha+\beta\right)\Gamma_1^{(2)} + \cos(\theta-\alpha+\beta)E_{ssp} + \cos(\theta-\alpha)E_{sps} + \cos(\beta)E_{pss}\right] \quad (11)$$

$$E_{ssp}(\omega_0) = \frac{ick_0^2}{2\pi|\hat{r}||\hat{I}|}\frac{e^{ik_0r_0}}{r_0}E_1(\omega_1)E_2(\omega_2)\cos\left(\frac{\theta}{2}-\alpha\right)\Gamma_2^{(2)}$$

$$E_{sps}(\omega_0) = \frac{ick_0^2}{2\pi|\hat{r}||\hat{I}|}\frac{e^{ik_0r_0}}{r_0}E_1(\omega_1)E_2(\omega_2)\cos\left(\frac{\theta}{2}-\alpha+\beta\right)\Gamma_3^{(2)}$$

$$E_{pss}(\omega_0) = \frac{ick_0^2}{2\pi|\hat{r}||\hat{I}|}\frac{e^{ik_0r_0}}{r_0}E_1(\omega_1)E_2(\omega_2)\cos\left(\frac{\theta}{2}\right)\Gamma_4^{(2)}$$

where i, j, k refer to the polarization state (s or p, see Figure 3a) of the SF, visible, and IR beams, respectively. The product $|\hat{r}||\hat{I}|$ is a unit vector product of a distance and current and is needed to preserve the units of eq 11. c is the speed of light. $\Gamma^{(2)}$ is the effective particle surface second-order susceptibility, which is

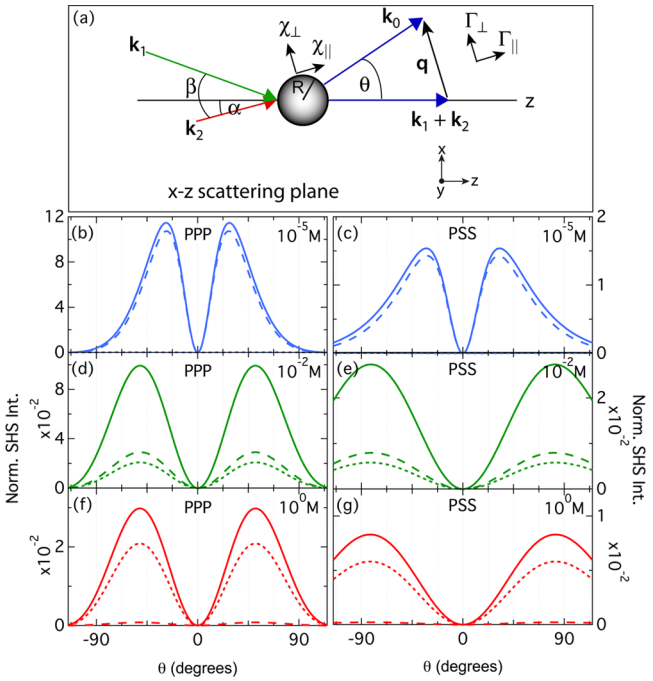

Figure 3. (a) Sketch of the SFS/SHS scattering geometry, top view. P-polarized light oscillates in the x-z (scattering) plane, while s-polarized light oscillates in the y direction. (b–g) Scattering patterns: (b, d, f) PPP and (c, e, g) PSS polarization combinations, calculated for a particle with $R = 50$ nm; (b, c) ionic strength of 10^{-5} M and $\Phi_0 = -286$ mV; (d, e) ionic strength of 10^{-2} M and $\Phi_0 = -109$ mV; (f, g) ionic strength of 1 M and $\Phi_0 = -21$ mV. Continuous lines are calculated assuming $\chi_{s,1}^{(2)} = 0$, $\chi_{s,2}^{(2)} = \chi_{s,3}^{(2)} = \chi_{s,4}^{(2)}$, $\chi_2^{(3)\prime} = \chi_3^{(3)\prime} = \chi_4^{(3)\prime}$, and $\chi_{s,2}^{(2)}/\chi_2^{(3)\prime} = -0.11$. The intensities originating from a pure surface response, $\chi^{(3)\prime} = 0$, and pure bulk response, $\chi_s^{(2)} = 0$, are displayed as dotted and dashed lines, respectively. The pure surface response (dotted lines) is the same for the same polarization independently from the ionic strength and surface potential.

defined as $\Gamma_{ijk}^{(2)} = \sum_{abc}\int_\Omega T_{ia}T_{jb}T_{kc}\chi_{s,abc}^{(2)}e^{i\mathbf{q}\cdot\mathbf{r}}\,d\Omega$, in which $\mathbf{r}$ is a point on the particle surface and the integration is performed on the overall surface Ω of the particle. This quantity captures the combined symmetry of the spherical scatterer and interacting electromagnetic fields. The $\Gamma_i^{(2)}$, $i = 1$–4, elements are defined as follows: $\Gamma_1^{(2)} = \Gamma_{\perp\perp\perp}^{(2)} - \Gamma_{\|\|\perp}^{(2)} - \Gamma_{\|\perp\|}^{(2)} - \Gamma_{\perp\|\|}^{(2)}$, $\Gamma_2^{(2)} = \Gamma_{\|\|\perp}^{(2)}$, $\Gamma_3^{(2)} = \Gamma_{\|\perp\|}^{(2)}$, and $\Gamma_4^{(2)} = \Gamma_{\perp\|\|}^{(2)}$. Here $\perp$ ($\|$) refers to the direction perpendicular (parallel) to $\mathbf{q}$. For noncliral surfaces, the effective susceptibility $\boldsymbol{\Gamma}^{(2)}$ is related to the surface susceptibility $\boldsymbol{\chi}_s^{(2)}$ by the following transformation:

$$\begin{pmatrix}\Gamma_1^{(2)}\\ \Gamma_2^{(2)}\\ \Gamma_3^{(2)}\\ \Gamma_4^{(2)}\end{pmatrix} = \begin{pmatrix}2F_1 - 5F_2 & 0 & 0 & 0\\ F_2 & 2F_1 & 0 & 0\\ F_2 & 0 & 2F_1 & 0\\ F_2 & 0 & 0 & 2F_1\end{pmatrix}\begin{pmatrix}\chi_{s,1}^{(2)}\\ \chi_{s,2}^{(2)}\\ \chi_{s,3}^{(2)}\\ \chi_{s,4}^{(2)}\end{pmatrix} \quad (12)$$

with $F_1(qR) = 2\pi R^2 i\left(\frac{\sin(qR)}{(qR)^2} - \frac{\cos(qR)}{qR}\right)$, and $F_2(qR) = 4\pi R^2 i\left(3\frac{\sin(qR)}{(qR)^4} - 3\frac{\cos(qR)}{(qR)^3} - \frac{\sin(qR)}{(qR)^2}\right)$.[48,51,52] Also $q = |\mathbf{q}|$, and R is the radius of the spherical particle; $\chi_{s,1}^{(2)} = \chi_{s,\perp\perp\perp}^{(2)} - \chi_{s,\|\|\perp}^{(2)} - \chi_{s,\|\perp\|}^{(2)} - \chi_{s,\perp\|\|}^{(2)}$, $\chi_{s,2}^{(2)} = \chi_{s,\|\|\perp}^{(2)}$, $\chi_{s,3}^{(2)} = \chi_{s,\|\perp\|}^{(2)}$, and $\chi_{s,4}^{(2)} = \chi_{s,\perp\|\|}^{(2)}$, where $\perp$ ($\|$) refers

DOI: 10.1021/acs.jpcc.5b12453
J. Phys. Chem. C 2016, 120, 9165–9173

to the direction perpendicular (parallel) to the particle surface. In the presence of an electrostatic field these expressions need to be modified,[50] similarly to the procedure for planar interfaces. This is done by replacing $\mathbf{\Gamma}^{(2)} \rightarrow \mathbf{\Gamma}^{(2)} + \mathbf{\Gamma}^{(3)\prime}$ with $\mathbf{\Gamma}^{(3)\prime}$, third-order effective particle susceptibility, defined as[50]

$$\Gamma_n^{(3)\prime} = \sum_{abc} \int_\Omega \int_R^{+\infty} T_{ia} T_{jb} T_{kc} \chi_n^{(3)\prime} E_{DC}(r) e^{i\mathbf{q}\cdot\mathbf{r}} \, dr \, d\Omega = \int_R^{+\infty} E_{DC}(r) \Gamma_n^{(3)}(r) \, dr \quad (13)$$

where $\Gamma_n^{(3)}(r) = 2F_1(qr)\chi_n^{(3)\prime}$ ($n = 2, 3, 4$) with $\chi_n^{(3)\prime}$ defined as in the case of planar interfaces. This simplification is possible because $E_{DC}(r)$ always points along the radial direction, and the integral over the angular range Ω is identical to that for $\mathbf{\Gamma}^{(2)}$. Eq 13 reduces to the same linear combination as reported in eq 12, however, because of symmetry properties $\chi_1^{(3)\prime} = \chi_{\perp\perp\perp,\perp}^{(3)\prime} - \chi_{\parallel\perp,\perp}^{(3)\prime} - \chi_{\parallel\perp\parallel,\perp}^{(3)\prime} - \chi_{\perp\parallel\parallel,\perp}^{(3)\prime} = 0$, and thus $\Gamma_1^{(3)\prime} = 0$. With $E_{DC}(r) = -\frac{d}{dr}\Phi(r)$, eq 13 can be rewritten as

$$\Gamma_n^{(3)\prime} = -\int_R^{+\infty} \frac{d\Phi(r)}{dr} \Gamma_n^{(3)}(r) \, dr \quad (14)$$

For ionic strengths >10^{-3} M, similar to the case of planar interfaces (Figure 1b), $E_{DC}(r)$ decays much faster than the period over which $\Gamma_n^{(3)}(r)$ varies, and thus, $\Gamma_n^{(3)}$ can be considered constant and equal to $\Gamma_n^{(3)}(R)$. Equation 14 then results in

$$\Gamma_n^{(3)\prime} = \Phi_0 \Gamma_n^{(3)}(R) = 2F_1(qR)\Phi_0\chi_n^{(3)\prime} \quad (15)$$

with Φ_0 the surface potential, in agreement with ref 50.

Interference and the Diffuse EDL. For ionic strengths <10^{-3} M we can imagine the particle as being surrounded by a soft shell (the diffuse EDL) with a thickness $4\kappa^{-1}$ over which $\Gamma_n^{(3)}(r)$ cannot be considered independent of r. In general eq 14 should be written as

$$\Gamma_n^{(3)\prime} = -\int_R^{+\infty} \frac{d\Phi(r)}{dr} \Gamma_n^{(3)}(r) \, dr = 2F_1(qR)\Phi_0\chi_n^{(3)\prime} + 2\chi_n^{(3)\prime} \int_R^{+\infty} \frac{dF_1(qr)}{dr} \Phi(r) \, dr \quad (16)$$

The second term now represents the contribution that originates from the diffuse EDL. As with eq 7, the second part of eq 16 only contributes to the expression several nanometers away from the interface. We can thus use $\Phi(r) = \Phi_0 \frac{R}{r} e^{-\kappa(r-R)}$, with $\Phi_0 = \Phi(R)$,[6] and obtain

$$\Gamma_n^{(3)\prime} = 2\Phi_0\chi_n^{(3)\prime}(F_1(qR) + F_3(\kappa R, qR)) \quad (17)$$

with $F_3(\kappa R, qR) = 2\pi R^2 i \frac{qR\cos(qR) + \kappa R \sin(qR)}{(qR)^2 + (\kappa R)^2}$, which depends on the particle radius R, the Debye length κ^{-1}, and the scattering wave vector modulus q. In the case of high ionic strength we have $\kappa^{-1} \rightarrow 0$ and $F_3(\kappa R, qR) \rightarrow 0$, in agreement with eq 15.[50] For low ionic strength, $\kappa \rightarrow 0$ and $F_3(\kappa R, qR) \rightarrow 2\pi R^2 i \frac{\cos(qR)}{qR}$, which modifies the scattering pattern. This behavior is different from the reflection and transmission mode experiments from planar interfaces (see Figure 2b) and offers an opportunity for gaining access to the EDL.

To demonstrate the effect of the $F_3(\kappa R, qR)$ term on SHS for different ionic strengths, we calculated SHS patterns for a spherical particle (R = 50 nm) in an aqueous solution containing either 10^{-5}, 10^{-2}, or 1 M of a 1:1 electrolyte as shown in Figure 3. For illustration purposes only, Φ_0 was calculated using[6,38] $\sigma_0 = \sqrt{8000 k_B T N_A c \varepsilon_0 \varepsilon_r}\left[\sinh\frac{e\Phi_0}{2k_BT} + \frac{1}{\varepsilon R}\sqrt{\frac{2k_BT\varepsilon_0\varepsilon_r}{1000c}}\tanh\frac{e\Phi_0}{4k_BT}\right]$ assuming a surface charge density $\sigma_0 = -0.05$ C/m^2 (the same as used for Figure 1). The solid lines show the resulting intensity scattering patterns (using the above equations and $\mathbf{\Gamma}^{(3)\prime}$ from eq 17), while the dotted and dashed lines represent the surface response ($\chi^{(3)\prime} = 0$) and the bulk response ($\chi_s^{(2)} = 0$), respectively. Note that the computed patterns for the individual contributions do not add up because we plot the intensities of the pure bulk and pure surface contribution omitting the cross product. It can be seen that the diffuse EDL contribution dominates for 10^{-5} M (Figure 3b,c) where it also strongly influences the shape of the scattering patterns. The intensity is much reduced for an ionic strength of 10^{-2} M (Figure 3d,e), and almost completely absent at 1 M (Figure 3f,g). There is thus a significant contribution from the diffuse EDL to the SHS pattern, especially for ionic strength <10^{-3} M. It is also important to note that the scattering patterns change significantly in shape. For the case of a scattering experiment, the $F_3(\kappa R, qR)$ contribution perturbs the $\chi^{(3)\prime}$ contribution, adds constructively to the $\chi^{(2)}$ contribution, and thus significantly distorts the shape of the scattering pattern resulting in a shift of the main peak toward forward scattering angles. In addition the peak shape is severely distorted, and it is distinctly different for different polarization combinations. This characteristic peak shape and polarization dependence should therefore be visible in particle/droplet dispersions with low ionic strength. We will test our theory using angle and polarization resolved SHS experiments of oil nanodroplets in ultrapure water.

Experimental Verification. Figure 4 shows angle-resolved SHS scattering patterns for two different polarization combinations (PPP and PSS) recorded from a dispersion of R = 75 nm hexadecane droplets stabilized with hexanol in ultrapure water. The ζ-potential of the droplets is −37 mV. The procedure for producing and characterizing the droplets as well

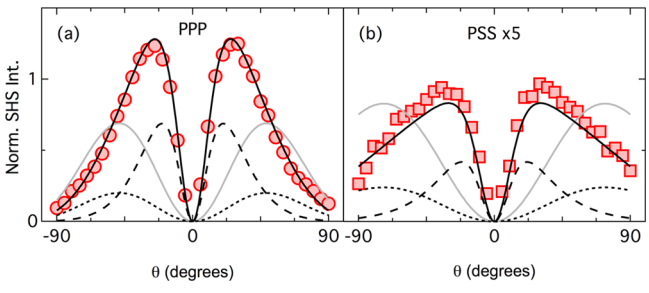

Figure 4. SHS intensity patterns of hexanol-covered hexadecane droplets in ultrapure water for (a) PPP and (b) PSS polarization combinations. The best fit (black line) was achieved using eq 17 for $\mathbf{\Gamma}^{(3)\prime}$, i.e., using the contribution of $F_3(\kappa R, qR)$ to describe the behavior at low ionic strength. The gray line represents the best fit without the $F_3(\kappa R, qR)$ correction, i.e., using eq 15 for $\mathbf{\Gamma}^{(3)\prime}$. The intensities originating from a pure surface response, $\chi^{(3)\prime} = 0$, and pure bulk response, $\chi_s^{(2)} = 0$, are displayed as dotted and dashed lines, respectively.

DOI: 10.1021/acs.jpcc.5b12453
J. Phys. Chem. C 2016, 120, 9165−9173

as the measurement and collection procedure for the SHS data are described in detail in ref 53. The black lines in Figure 4 are fits for both the PPP and PSS data obtained using eqs 10 and 11 replacing $\mathbf{\Gamma}^{(2)} \rightarrow \mathbf{\Gamma}^{(2)} + \mathbf{\Gamma}^{(3)\prime}$ with $\mathbf{\Gamma}^{(3)\prime}$ from eq 17, with R = 75 nm (as obtained from dynamic light scattering), $1/\kappa$ = 168 nm ($c = 3.32 \times 10^{-6}$ mol/L), and $\chi^{(2)}_{s,2}/(\chi^{(3)\prime}_{2}\Phi_0) = 3.8$, assuming $\chi^{(2)}_{s,2} = \chi^{(2)}_{s,3} = \chi^{(2)}_{s,4}$ and $\chi^{(2)}_{s,1} = 0$ and $\chi^{(3)}_{2} = \chi^{(3)}_{3} = \chi^{(3)}_{4}$.[48] It can be seen that the black lines represent the data very well. The scattering patterns can be broken down into a surface ($\chi^{(2)}_{s}$ only) and diffuse EDL ($\chi^{(3)\prime}$ only) contribution. From this procedure it can be determined that 55% of the total emitted field from this sample originates from the diffuse EDL. The gray line is the fit that would be obtained using $\mathbf{\Gamma}^{(3)\prime}$ from eq 15 (without the diffuse EDL contribution). This curve does not capture the typical asymmetric shape of the scattering pattern and peaks at a larger scattering angle indicative of an underestimation of the size of the soft shell around the droplets. We thus find that adding interference, which takes place inside the diffuse EDL, to the scattering formalism describes the patterns at ionic strengths $<10^{-3}$ M very accurately. It is also clear that for the case of scattering that the angle and polarization resolved data represent a way to determine surface properties in a very accurate manner. In comparison to a curve plotting intensity versus concentration as is the norm for reflection experiments, the scattering patterns are very sensitive to the state of the EDL. Thus, instead of probing an ionic strength series, polarization specific scattering patterns offer a much bigger opportunity to assess the physicochemical properties of the EDL.

Comparison between Reflection, Transmission, and Scattering Experiments. Turning now our attention to the difference between scattering and reflection/transmission experiment, we note the following differences:

(1) Scattering and reflection/transmission experiments are described by a completely different set of equations reflecting the different optical processes taking place in the different systems. These equations are solutions to the Maxwell equations that depend on the geometry and topology of the light−matter interaction process. Just like in linear scattering and reflection/transmission experiments where the former is, e.g., described by Rayleigh scattering or Mie scattering and the latter is described by the Fresnel factors, each process needs to be described with the physical expressions that report the right type of light−matter interactions. This means that also for nonlinear optical processes it is not meaningful to describe an intensity versus ionic strength series by eq 4 (or eq 9).

(2) There is a distinct difference in ionic strength dependence. To illustrate this, we compare the concentration dependence by examining $|f_3(\kappa, \Delta k_z)|$ in reflection geometry in Figure 2a and $|F_3(\kappa R, qR)|/(4\pi R^2)$ for a particle with R = 50 nm in scattering geometry in Figure 2b. Note that here there is no polarization dependence yet. While $|f_3(\kappa, \Delta k_z)|$ is small for $c < 10^{-3}$ M, and increases at higher ionic strengths, $|F_3(\kappa R, qR)|/(4\pi R^2)$ is large for $c < 10^{-3}$ M and vanishes at higher ionic strength. In the ionic strength range from 10^{-7} M to 10^{-3} M, the reflected intensity increases with increasing ionic strength while the scattering intensity decreases. A more important difference, however, originates from the dependence on the scattering angle. Figure 2b shows $|F_3(\kappa R, qR)|/(4\pi R^2)$ for scattering angles of 10°, 45°, and 80°. It can be seen that the magnitude of $|F_3(\kappa R, qR)|/(4\pi R^2)$ at low ionic strength either continuously decreases with ionic strength (10°), or remains relatively level and then decreases (45°), or increases to a maximum and then decreases (80°). This behavior translates directly into an intensity dependence that would qualitatively follow those trends.

(3) Different polarization combinations result in different scattering pattern shapes. This offers an opportunity for a more extensive characterization of the EDL than what is possible at planar interfaces.

(4) As mentioned the dependence on the scattering angle offers a unique opportunity to characterize the EDL. As previously pointed out,[54] measuring SHS in the forward direction is not the optimal way of gathering SHS light that exclusively originates from the surface. This is clearly shown in this work as well, in Figures 3 and 4.

Scanning the detection angle and changing the polarization combination are not important parameters for reflection/transmission mode experiments, and probably for this reason they have not been considered relevant for the measurement and description of particle interfaces.[11,26,28,55,56] A typical procedure to examine the surface of particles in solution is to record the SHG intensity in the forward direction. Typically, the SHG intensity shows a continuously decreasing trend with ionic strength that is then described by eq 4 employing the Gouy−Chapman model (or variations thereof). While values for a surface potential and charge density can be derived in this way, the description is made using a solution for an unrelated problem (namely, a reflection experiment, (1) in the above list). Therefore, the solutions are not physically meaningful.

It can be shown via another argumentation that the obtained surface potential values are ambiguous. The computation values for $|F_3(\kappa R, qR)|/(4\pi R^2)$ in Figure 2b are approximately proportional to the square root of the intensity ($\sqrt{I}$). The curves show that the same particle dispersion can produce a different $\sqrt{I}$ versus c curve simply by selecting a different scattering angle (in the case of Figure 2b, θ = 10°, 45°, and 80°). If the acceptance angle of the detected SHG light or the central scattering angle had been different, a fit with eq 4 would have returned a different surface potential as a result.

To illustrate agreement with our model we have also calculated the expected intensity versus concentration behavior for one of the data sets in the literature (Figure 6 of ref 55). The figure is reported in the Supporting Information (Figure S1), together with a calculation using eqs 10, 11, and 17. It can be seen that good agreement between the experimental data and our model is achieved.

■ CONCLUSIONS

In summary, we have described theoretical SFG/SHG experiments in reflection, transmission, and scattering modes considering explicitly the effects of low and high ionic strength on the emitted light. If an electrostatic field is present in the interfacial region, it will contribute to the intensity. For low ionic strengths ($<10^{-3}$ M) the diffuse EDL can lead to significant distortions to the emitted light (compared to the case of higher ionic strengths) because of an interference between SHG/SFG photons that are generated at different positions within the EDL. For reflection and scattering mode experiments in typical experimental conditions, this interference can give rise to a probing depth up to ∼1 μm instead of being restricted to a region smaller than 1 nm. The described effect significantly modifies the interpretation of ion dependent SHG/SFG data. SHG and SFG scattering measurements in principle report on the same phenomenon as their planar geometry counterparts but contain a broader range of

DOI: 10.1021/acs.jpcc.5b12453
J. Phys. Chem. C 2016, 120, 9165−9173

parameters that can be varied (scattering angle, particle size, polarization state of the light). Here the diffuse EDL takes the shape of a soft shell that not only produces a change in the scattered intensity but also significantly distorts the angle-resolved scattering pattern, which is different for different polarization combinations. Comparing the derived scattering model to SHS scattering data obtained from hexanol-covered hexadecane nanodroplets in water, we are able to describe the scattering patterns for different polarization combinations without making any assumptions about the surface.

The presented description is only relevant insofar as the main aqueous phase is probed, i.e., for vibrational SFG experiments that center on the O−H stretch or bending mode (e.g., reviewed in ref 57), resonant SHG experiments that focus on the charge transfer to solvent mode insofar the water is also resonantly excited (e.g., ref 58), and nonresonant SHG measurements that probe the response of all noncentrosymmetric molecules in the sample (e.g., refs 11 and 59−61).

Given the interest and relevance of the electrostatic properties of interfaces and the need to characterize their properties,[38] our results are of great value for determining the structure and properties of the EDL of aqueous interfaces. In the case of SH and SF scattering, it can be seen that the polarization dependent scattering patterns are very sensitive to the shape of the additional form factor $F_3(\kappa R, qR)$. This opens up future avenues for determining the surface potential without assumptions about the structure and properties of the EDL.

■ ASSOCIATED CONTENT

Supporting Information

The Supporting Information is available free of charge on the ACS Publications website at DOI: 10.1021/acs.jpcc.5b12453.

Comparison of our scattering theory with data from Figure 6 from ref 55 (PDF)

■ AUTHOR INFORMATION

Corresponding Author

*E-mail: sylvie.roke@epfl.ch.

Author Contributions

#G.G. and C.L. contributed equally.

Notes

The authors declare no competing financial interest.

■ ACKNOWLEDGMENTS

This work is supported by the Julia Jacobi Foundation, and the European Research Council (Grants 240556 and 616305). G.G. acknowledges the Donors of the American Chemical Society Petroleum Research Fund for partial support in the initial stages of this research (Grant 52618-ND6) and Ellen Backus, Mischa Bonn, Johannes Hunger, Yuki Nagata, and Eric Tyrode for helpful discussion.

■ REFERENCES

(1) Zhang, Y. J.; Cremer, P. S. Interactions between Macromolecules and Ions: The Hofmeister Series. *Curr. Opin. Chem. Biol.* **2006**, *10*, 658−663.

(2) Jubb, A. M.; Hua, W.; Allen, H. C. Environmental Chemistry at Vapor/Water Interfaces: Insights from Vibrational Sum Frequency Generation Spectroscopy. *Annu. Rev. Phys. Chem.* **2012**, *63*, 107−130.

(3) Marcus, Y. Effect of Ions on the Structure of Water: Structure Making and Breaking. *Chem. Rev.* **2009**, *109*, 1346−1370.

(4) Tobias, D. J.; Stern, A. C.; Baer, M. D.; Levin, Y.; Mundy, C. J. Simulation and Theory of Ions at Atmospherically Relevant Aqueous Liquid-Air Interfaces. *Annu. Rev. Phys. Chem.* **2013**, *64*, 339−359.

(5) Hunter, R. J. *Zeta Potential in Colloid Science*; Academic Press: Sydney, 1981.

(6) Oshima, H. *Theory of Colloid and Interfacial Phenomena*; Academic Press, 2006.

(7) Melnichenko, Y. *Small-Angle Scattering from Confined and Interfacial Fluids*, 1st ed.; Springer International Publishing, 2016; p 314.

(8) Jungwirth, P.; Finlayson-Pitts, B. J.; Tobias, D. J. Introduction: Structure and Chemistry at Aqueous Interfaces. *Chem. Rev.* **2006**, *106*, 1137−1139.

(9) Johnson, C. M.; Baldelli, S. Vibrational Sum Frequency Spectroscopy Studies of the Influence of Solutes and Phospholipids at Vapor/Water Interfaces Relevant to Biological and Environmental Systems. *Chem. Rev.* **2014**, *114*, 8416−8446.

(10) Salmeron, M.; Schlogl, R. Ambient Pressure Photoelectron Spectroscopy: A New Tool for Surface Science and Nanotechnology. *Surf. Sci. Rep.* **2008**, *63*, 169−199.

(11) Eisenthal, K. B. Second Harmonic Spectroscopy of Aqueous Nano- and Microparticle Interfaces. *Chem. Rev.* **2006**, *106*, 1462−1477.

(12) Eisenthal, K. B. Liquid Interfaces Probed by Second-Harmonic and Sum-Frequency Spectroscopy. *Chem. Rev.* **1996**, *96*, 1343−1360.

(13) Jungwirth, P.; Winter, B. Ions at Aqueous Interfaces: From Water Surface to Hydrated Proteins. *Annu. Rev. Phys. Chem.* **2008**, *59*, 343−366.

(14) Geiger, F. M. Second Harmonic Generation, Sum Frequency Generation, and Chi(3): Dissecting Environmental Interfaces with a Nonlinear Optical Swiss Army Knife. *Annu. Rev. Phys. Chem.* **2009**, *60*, 61−83.

(15) Abel, B. Hydrated Interfacial Ions and Electrons. *Annu. Rev. Phys. Chem.* **2013**, *64*, 533−552.

(16) Eftekhari-Bafrooei, A.; Borguet, E. Effect of Electric Fields on the Ultrafast Vibrational Relaxation of Water at a Charged Solid-Liquid Interface as Probed by Vibrational Sum Frequency Generation. *J. Phys. Chem. Lett.* **2011**, *2*, 1353−1358.

(17) Ong, S.; Zhao, X.; Eisenthal, K. B. Polarization of Water Molecules at a Charged Interface: Second Harmonic Studies of the Silica/Water Interface. *Chem. Phys. Lett.* **1992**, *191*, 327−335.

(18) Tian, C. S.; Shen, Y. R. Structure and Charging of Hydrophobic Material/Water Interfaces Studied by Phase-Sensitive Sum-Frequency Vibrational Spectroscopy. *Proc. Natl. Acad. Sci. U. S. A.* **2009**, *106*, 15148−15153.

(19) Willard, A. P.; Chandler, D. Instantaneous Liquid Interfaces. *J. Phys. Chem. B* **2010**, *114*, 1954−1958.

(20) Jena, K. C.; Covert, P. A.; Hore, D. K. The Effect of Salt on the Water Structure at a Charged Solid Surface: Differentiating Second- and Third-Order Nonlinear Contributions. *J. Phys. Chem. Lett.* **2011**, *2*, 1056−1061.

(21) Richmond, G. L. Molecular Bonding and Interactions at Aqueous Surfaces as Probed by Vibrational Sum Frequency Spectroscopy. *Chem. Rev.* **2002**, *102*, 2693−2724.

(22) Shen, Y. R. Surface Properties Probed by Second-Harmonic and Sum-Frequency Generation. *Nature* **1989**, *337*, 519−519.

(23) Gragson, D. E.; McCarty, B. M.; Richmond, G. L. Ordering of Interfacial Water Molecules at the Charged Air/Water Interface Observed by Vibrational Sum Frequency Generation. *J. Am. Chem. Soc.* **1997**, *119*, 6144−6152.

(24) Shen, Y. R.; Ostroverkhov, V. Sum-Frequency Vibrational Spectroscopy on Water Interfaces: Polar Orientation of Water Molecules at Interfaces. *Chem. Rev.* **2006**, *106*, 1140−1154.

(25) Piatkowski, L.; Zhang, Z.; Backus, E. H. G.; Bakker, H. J.; Bonn, M. Extreme Surface Propensity of Halide Ions in Water. *Nat. Commun.* **2014**, *5*, 4083.

(26) Yan, E. C. Y.; Liu, Y.; Eisenthal, K. B. New Method for Determination of Surface Potential of Microscopic Particles by Second Harmonic Generation. *J. Phys. Chem. B* **1998**, *102*, 6331−6336.

DOI: 10.1021/acs.jpcc.5b12453
J. Phys. Chem. C 2016, 120, 9165−9173

(27) Gomopoulos, N.; Lutgebaucks, C.; Sun, Q. C.; Macias-Romero, C.; Roke, S. Label-Free Second Harmonic and Hyper Rayleigh Scattering with High Efficiency. *Opt. Express* **2013**, *21*, 815−821.
(28) Sauerbeck, C.; Braunschweig, B.; Peukert, W. Surface Charging and Interfacial Water Structure of Amphoteric Colloidal Particles. *J. Phys. Chem. C* **2014**, *118*, 10033−10042.
(29) Schurer, B.; Wunderlich, S.; Sauerbeck, C.; Peschel, U.; Peukert, W. Probing Colloidal Interfaces by Angle-Resolved Second Harmonic Light Scattering. *Phys. Rev. B: Condens. Matter Mater. Phys.* **2010**, *82*, 241404R.
(30) Boyd, R. W. *Nonlinear Optics*, 3rd ed.; Academic Press: Amsterdam, 2008; p 613.
(31) Zhao, X.; Ong, S.; Eisenthal, K. B. Polarization of Water Molecules at a Charged Interface. Second Harmonic Studies of Charged Monolayers at the Air/Water Interface. *Chem. Phys. Lett.* **1993**, *202*, 513−520.
(32) Roke, S.; Gonella, G. Nonlinear Light Scattering and Spectroscopy of Particles and Droplets in Liquids. *Annu. Rev. Phys. Chem.* **2012**, *63*, 353−78.
(33) de Beer, A. G. F.; Campen, R. K.; Roke, S. Separating Surface Structure and Surface Charge with Second-Harmonic and Sum-Frequency Scattering. *Phys. Rev. B: Condens. Matter Mater. Phys.* **2010**, *82*, 235431.
(34) Shen, Y. R. *The Principles of Nonlinear Optics*, Wiley Classics Library ed.; Wiley-Interscience: Hoboken, NJ, 2003; p 563.
(35) Sokhan, V. P.; Tildesley, D. J. Molecular Dynamics Simulation of the Non-Linear Optical Susceptibility at the Phenol/Water/Air Interface. *Faraday Discuss.* **1996**, *104*, 193−208.
(36) Sokhan, V. P.; Tildesley, D. J. The Free Surface of Water: Molecular Orientation, Surface Potential and Nonlinear Susceptibility. *Mol. Phys.* **1997**, *92*, 625−640.
(37) Goh, M. C.; Hicks, J. M.; Kemnitz, K.; Pinto, G. R.; Bhattacharyya, K.; Heinz, T. F.; Eisenthal, K. B. Absolute Orientation of Water-Molecules at the Neat Water-Surface. *J. Phys. Chem.* **1988**, *92*, 5074−5075.
(38) Hunter, R. J. *Foundations of Colloid Science*; Oxford University Press, 2001.
(39) Ishiyama, T.; Morita, A. Molecular Dynamics Study of Gas-Liquid Aqueous Sodium Halide Interfaces. Ii. Analysis of Vibrational Sum Frequency Generation Spectra. *J. Phys. Chem. C* **2007**, *111*, 738−748.
(40) Tian, C. S.; Ji, N.; Waychunas, G. A.; Shen, Y. R. Interfacial Structures of Acidic and Basic Aqueous Solutions. *J. Am. Chem. Soc.* **2008**, *130*, 13033−13039.
(41) Samson, J. S.; Scheu, R.; Smolentsev, N.; Rick, S. W.; Roke, S. Sum Frequency Spectroscopy of the Hydrophobic Nanodroplet/Water Interface: Absence of Hydroxyl Ion and Dangling OH Bond Signatures. *Chem. Phys. Lett.* **2014**, *615*, 124−131.
(42) Tian, C. S.; Byrnes, S. J.; Han, H. L.; Shen, Y. R. Surface Propensities of Atmospherically Relevant Ions in Salt Solutions Revealed by Phase-Sensitive Sum Frequency Vibrational Spectroscopy. *J. Phys. Chem. Lett.* **2011**, *2*, 1946−1949.
(43) Zhang, L.; Tian, C.; Waychunas, G. A.; Shen, Y. R. Structures and Charging of Alpha-Alumina (0001)/Water Interfaces Studied by Sum-Frequency Vibrational Spectroscopy. *J. Am. Chem. Soc.* **2008**, *130*, 7686−7694.
(44) Achtyl, J. L.; Vlassiouk, I. V.; Fulvio, P. F.; Mahurin, S. M.; Dai, S.; Geiger, F. M. Free Energy Relationships in the Electrical Double Layer over Single-Layer Graphene. *J. Am. Chem. Soc.* **2013**, *135*, 979−981.
(45) Strazdaite, S.; Versluis, J.; Bakker, H. J. Water Orientation at Hydrophobic Interfaces. *J. Chem. Phys.* **2015**, *143*, 084708.
(46) Ye, S.; Nihonyanagi, S.; Uosaki, K. Sum Frequency Generation (Sfg) Study of the Ph-Dependent Water Structure on a Fused Quartz Surface Modified by an Octadecyltrichlorosilane (Ots) Monolayer. *Phys. Chem. Chem. Phys.* **2001**, *3*, 3463−3469.
(47) Agmon, N.; Bakker, H. J.; Campen, R. K.; Henchman, R.; Pohl, P.; Roke, S.; Thame, M.; Hassanali, A. Protons and Hydroxide Ions in Aqueous Systems. *Chem. Rev.* **2016**, *116*, submitted.
(48) de Beer, A. G. F.; Roke, S. Obtaining Molecular Orientation from Second Harmonic and Sum Frequency Scattering Experiments: Angular Distribution and Polarization Dependence. *J. Chem. Phys.* **2010**, *132*, 234702−234708.
(49) Roke, S.; Gonella, G. Nonlinear Light Scattering and Spectroscopy of Particles and Droplets in Liquids. *Annu. Rev. Phys. Chem.* **2012**, *63*, 353−378.
(50) de Beer, A. G. F.; Campen, R. K.; Roke, S. Separating Surface Structure and Surface Charge with Second-Harmonic and Sum-Frequency Scattering. *Phys. Rev. B: Condens. Matter Mater. Phys.* **2010**, *82*, 235431−235431.
(51) Roke, S.; Bonn, M.; Petukhov, A. V. Nonlinear Optical Scattering: The Concept of Effective Susceptibility. *Phys. Rev. B: Condens. Matter Mater. Phys.* **2004**, *70*, 115106.
(52) Roke, S.; Roeterdink, W. G.; Wijnhoven, J. E. G. J.; Petukhov, A. V.; Kleyn, A. W.; Bonn, M. Vibrational Sum Frequency Scattering from a Submicron Suspension. *Phys. Rev. Lett.* **2003**, *91*, 258302.
(53) Chen, Y. X.; Jena, K. C.; Roke, S. From Hydrophobic to Hydrophilic: The Structure and Density of the Hexadecane Droplet/Alkanol/Water Interface. *J. Phys. Chem. C* **2015**, *119*, 17725−17734.
(54) Dadap, J. I.; Shan, J.; Eisenthal, K. B.; Heinz, T. F. Second-Harmonic Rayleigh Scattering from a Sphere of Centrosymmetric Material. *Phys. Rev. Lett.* **1999**, *83*, 4045−4048.
(55) Campen, R. K.; Pymer, A. K.; Nihonyanagi, S.; Borguet, E. Linking Surface Potential and Deprotonation in Nanoporous Silica: Second Harmonic Generation and Acid/Base Titration. *J. Phys. Chem. C* **2010**, *114*, 18465−18473.
(56) Kumal, R. R.; Karam, T. E.; Haber, L. H. Determination of the Surface Charge Density of Colloidal Gold Nanoparticles Using Second Harmonic Generation. *J. Phys. Chem. C* **2015**, *119*, 16200−16207.
(57) Bonn, M.; Nagata, Y.; Backus, E. H. G. Molecular Structure and Dynamics of Water at the Water-Air Interface Studied with Surface-Specific Vibrational Spectroscopy. *Angew. Chem., Int. Ed.* **2015**, *54*, 5560−5576.
(58) Petersen, P. B.; Saykally, R. J. Adsorption of Ions to the Surface of Dilute Electroyte Solutions: The Jones-Ray Effect Revisited. *J. Am. Chem. Soc.* **2005**, *127*, 15446−15452.
(59) Scheu, R.; Rankin, B. M.; Chen, Y. X.; Jena, K. C.; Ben-Amotz, D.; Roke, S. Charge Asymmetry at Aqueous Hydrophobic Interfaces and Hydration Shells. *Angew. Chem., Int. Ed.* **2014**, *53*, 9560−9563.
(60) Scheu, R.; Chen, Y. X.; de Aguiar, H. B.; Rankin, B. M.; Ben-Amotz, D.; Roke, S. Specific Ion Effects in Amphiphile Hydration and Interface Stabilization. *J. Am. Chem. Soc.* **2014**, *136*, 2040−2047.
(61) Scheu, R.; Chen, Y. X.; Subinya, M.; Roke, S. Stern Layer Formation Induced by Hydrophobic Interactions: A Molecular Level Study. *J. Am. Chem. Soc.* **2013**, *135*, 19330−19335.

DOI: 10.1021/acs.jpcc.5b12453
J. Phys. Chem. C 2016, 120, 9165−9173